Research Article | Vol. 32, No. 16 / 29 Jul 2024 / Optics Express 28644
Optics EXPRESS

Fast spectroscopic imaging using extreme ultraviolet interferometry

HANNAH C. STRAUCH,[1] FENGLING ZHANG,[2] STEFAN MATHIAS,[1] THORSTEN HOHAGE,[3] STEFAN WITTE,[2] AND G. S. MATTHIJS JANSEN[1,*]

[1] *1st Institute of Physics, University of Göttingen, Germany*
[2] *Advanced Research Center for Nanolithography ARCNL, Amsterdam, The Netherlands*
[3] *Institute for Numerical and Applied Mathematics, University of Göttingen, Germany*
[*] *gsmjansen@uni-goettingen.de*

Abstract: Extreme ultraviolet pulses as generated by high harmonic generation (HHG) are a powerful tool for both time-resolved spectroscopy and coherent diffractive imaging. However, the integration of spectroscopy and microscopy to harness the unique broadband spectra provided by HHG is hardly explored due to the challenge to decouple spectroscopic and microscopic information. Here, we present an interferometric approach to this problem that combines Fourier transform spectroscopy (FTS) with Fourier transform holography (FTH). This is made possible by the generation of phase-locked pulses using a pair of HHG sources. Crucially, in our geometry the number of interferometric measurements required is at most equal to the number of high-harmonics in the illumination, and can be further reduced by incorporating prior knowledge about the structure of the FTH sample. Compared to conventional FTS, this approach achieves over an order of magnitude increase in acquisition speed for full spectro-microscopic data, and furthermore allows high-resolution computational imaging.

1. Introduction

Coherent extreme ultraviolet light produced by high-harmonic generation [1] provides a unique opportunity for the study of ultrafast dynamics in condensed matter at the nanoscale. On the one hand, the short wavelength yields a favourable Abbe resolution limit, and extreme ultraviolet (EUV) coherent diffractive imaging (CDI) nowadays enables imaging at nanometer-scale resolution [2–4]. On the other hand, the wide range of photon energies and ultrashort, attosecond (as) to femtosecond (fs) pulse durations of EUV light pulses from high-harmonic generation (HHG) provide access to a wide range of elemental absorption edges. Here, time-resolved spectroscopy yields a sensitive element-resolved probe of dynamics of the electrons, the spins and the lattice in optically excited matter [5–11]. The combination of both these approaches, namely nanometer-scale microscopic time-resolved EUV spectroscopy, is highly appealing, as it would enable the study of complex dynamics in nanoscale structures ranging from naturally-inhomogeneous quantum materials to fabricated heterostructures. However, such multi-dimensional measurements remain out of reach for HHG light sources as is, and can so far only be performed at significant experimental cost at accelerator-based EUV light sources [12,13].

Holography plays an important role in the development of advanced EUV microscopy [14–19]. For example, time-resolved EUV microscopy is commonly performed by combining Fourier-transform holography (FTH) with numerical phase retrieval [13,20]. In FTH, the diffracted wave from the sample is interfered with a reference wave that is generated by a point-like structure (usually a pinhole in transmission geometry). The resulting fringe pattern in the far-field diffraction pattern allows for direct image reconstruction by a single Fourier transform. The single-shot nature of the FTH measurement is critical for the implementation of time-resolved

#523102 https://doi.org/10.1364/OE.523102
Journal © 2024 Received 6 Mar 2024; revised 13 Jun 2024; accepted 13 Jun 2024; published 25 Jul 2024

Optics EXPRESS

studies, as it implies that only the pump-probe delay needs to be scanned during an experiment. In contrast, ptychography is a powerful imaging method that enables diffraction-limited resolution and can handle experimental challenges such as partial coherence, multi-spectral illumination and structured illumination profiles [2,21–23]. To achieve this, ptychography relies on spatial scanning of the sample in overlapping steps such that the phase retrieval problem is sufficiently constrained. The need for overlap is significantly increased for multi-spectral illumination [2,22,24]. A full time- and spectrum-resolved ptychography measurement would therefore place significant requirements on the brightness and stability of the EUV light source. Thus, there is a clear need for a fast spectromicroscopy technique that reduces the data collection time for scanning in the spatial and spectral domains.

A promising alternative approach to solve this challenge is EUV Fourier transform spectroscopy (FTS) [25–28] using a pair of phase-locked HHG sources. Spatially resolved FTS enables spectral multiplexing: the full HHG spectrum can be used for imaging with no requirements or assumptions on the spectral response of the sample [28–30]. Since spectral resolution is achieved by interferometric delay scanning, however, it is not clear that the multiplexing advantage also leads to an increase in data acquisition rate. Moreover, it is unclear how the two spatially separated HHG beams can be focused to the sample to make efficient use of the generated EUV flux.

In this article, we demonstrate Fourier-transform spectroscopic holography (FTSH) (Fig. 1), which combines FTH with an interferometric FTS measurement. This directly improves photon

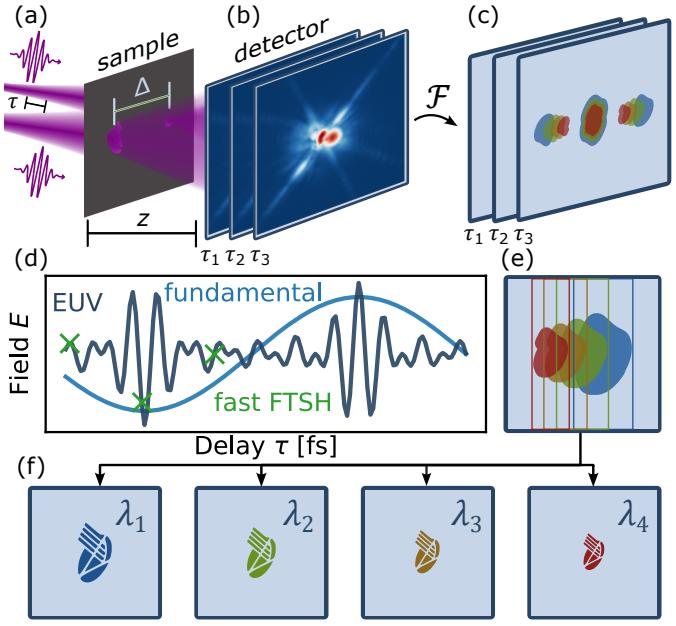

Fig. 1. Overview of the Fourier transform spectroscopic holography (FTSH) workflow. (a) Two phase-locked polychromatic EUV beams from a pair of HHG sources illuminate the sample and reference structures. (b) The diffraction pattern is detected by a camera in the far-field. (c) As in conventional FTH, a single Fourier transform is used to analyze the interference pattern, however in this case the holograms of the individual photon energies are superimposed. (d) By time-shifting the reference wave, Fourier transform spectroscopy allows to measure the spectrum at each pixel. The necessary sampling for this measurement is significantly reduced when the multi-wavelength nature of the hologram (e) is considered, as the different spectral components are only partially overlapping. Thus, an HHG spectrum with N_λ harmonics requires at most N_λ and typically less measurements to fully recover a spectrally-resolved image (f).

Optics EXPRESS

efficiency, as the EUV beams can be focused to the sample and reference structures individually. More interestingly, we also find that this combination enables a direct reduction in experimental scanning: For an HHG spectrum with N_λ harmonics, FTSH requires at most N_λ measurements and this number can be further reduced by incorporating prior knowledge of the sample structure. To achieve this, we exploit the intrinsic coupling between spectral and spatial information in the FTH diffraction pattern. For our HHG spectrum (covering up to 11 harmonics from 80 to 29 nm, see Fig. 2(c)) and sample geometry, we find that only 6 phase steps are necessary to recover all spectral components completely.

2. Theory

Fourier-transform spectroscopic holography (Fig. 1) can be understood as an extension of FTH towards multiple wavelengths. For a single wavelength λ_i, the far-field diffraction pattern of an FTH sample can be expressed as $I_{\lambda_i}(k) = |\tilde{p}_i|^2 + |\tilde{r}_i|^2 + \tilde{p}_i\tilde{r}_i^* + \tilde{p}_i^*\tilde{r}_i$, where $\tilde{p}$ and $\tilde{r}$ are the electric fields at the detection plane due to the probed sample and reference, respectively, while k is the spatial frequency of the scattered wave. The fields $\tilde{p}$ and $\tilde{r}$ can be related to the fields p and r at the sample plane by optical propagation. For Fraunhofer diffraction, the propagation is given by a scaled Fourier transform, where the scale (i.e., the extent of the diffraction pattern on the camera) is proportional to the wavelength of illumination. Consequently, a Fourier transform ($\mathcal{F}$)

$$\mathcal{F}\{I_{\lambda_i}\}(x) = \; p_i * p_i^* + r_i * r_i^* + p_i * r_i^* + p_i^* * r_i \tag{1}$$

provides direct access to the holograms ($p_i * r_i^*$ and $p_i^* * r_i$) in the real-space coordinates x. It is well known that the resolution of these holograms is limited by the size of the reference r, and furthermore that the hologram appears separated from the autocorrelation terms ($p_i * p_i^*$ and $r_i * r_i^*$) at a distance Δ from the center that is equal to to the separation of p and r. In terms of pixels of the reconstructed image, the separation becomes $\Delta_{\mathrm{px}} = \Delta D/\lambda z$, where z is the distance and D the size of the detector. Notably, the numerical hologram separation Δ_{px} is inversely proportional to the wavelength as a consequence of the wavelength scaling of the Fraunhofer propagation operator.

While the precise position of the hologram in the frame is not important in monochromatic FTH, it becomes relevant for spectrally-resolved applications. If an FTH hologram is recorded using polychromatic radiation, a spatial Fourier transform of the data yields an image where the individual holograms are shifted according to the illuminating wavelength. This effect has been harnessed to perform single-shot spectrally resolved FTH using the individual high harmonics of a HHG light source [31]. However, this requires a specific experimental geometry: in order to fully separate the individual holograms, the sample width needs to be reduced significantly (or equivalently the Δ must be increased) by a factor that depends on the wavelength difference of neighbouring high harmonics. This drastically reduces the achievable field of view and limits the spectral resolution, altogether preventing the application to continuous (attosecond) EUV spectra. Therefore, another method is necessary to resolve the individual spectral components.

Fourier transform spectroscopy (FTS) is a powerful method that provides such a capability: analogous to FTH, interference of two pulses delayed in the time domain gives access to the spectrum by an inverse Fourier transform. FTS-based methods are already commonly used to perform hyperspectral imaging in the visible and infrared ranges (e.g., [32,33]). In the last decade, FTS at extreme ultraviolet wavelengths has been enabled by the generation of phase-locked EUV pulse pairs by phase-locked laser pulses [27,28]. Integrated in a CDI experiment, spatially-resolved FTS yields monochromatic diffraction patterns that can be used for numerical image reconstruction [30]. In order to satisfy the Nyquist-Shannon sampling theorem and to accurately measure the complete spectrum, however, typically a few hundred interferometric diffraction patterns at different delays must be measured.

Optics EXPRESS

Here, we show that the individual limitations of FTH and FTS can be lifted when they are combined in a HHG-based interferometric measurement (cf. Fig. 1). In particular, we propose to combine the FTSH measurement with prior knowledge of the experimental parameters. The generated wavelengths of a HHG source are generally known in advance to a good accuracy, e.g., from a prior spectroscopy measurement or from a measurement of the fundamental laser parameters. This knowledge can already significantly reduce the sampling requirements, but a further reduction is possible: Combined with knowledge of the FTH mask structure, it is possible to calculate which spectral components can contribute to each pixel in the FTH hologram. For comb-like HHG spectra spanning an octave or more, it is generally found that only a small number of harmonics contribute to each pixel in the multi-wavelength hologram.

It is instructive to consider the following example: an FTH sample containing a reference structure with negligible width and a sample with width W (along the sample-reference direction) with a sample-reference separation $\Delta = 2W$ is illuminated by a HHG spectrum containing the 9 odd harmonics 13 to 29 of a 1030 nm driving laser. In this case, the hologram of the 29$^{\text{th}}$ harmonic has significant overlap with the 27$^{\text{th}}$, successively less overlap with the 25$^{\text{th}}$, 23$^{\text{rd}}$ and 21$^{\text{st}}$ harmonic holograms, and no overlap with holograms of the 19$^{\text{th}}$ and lower high harmonics. In fact, no more than 6 high harmonics overlap at any point in the multi-wavelength hologram. This suggests that the sampling requirements in an FTS measurement can be reduced.

In FTSH, the reference beam is delayed by a time τ with respect to the probe beam. This leads to a measured intensity given by $I(k,\tau) = \sum_i^{N_\lambda} |\tilde{p}_i + \tilde{r}_i e^{-i2\pi c\tau/\lambda_i}|^2$. By applying a Fourier transform, we can express the measured multi-wavelength hologram $M(x',T)$ as

$$M(x',\tau) = \sum_i^{N_\lambda} p_i * p_i^* + r_i * r_i^* + (p_i * r_i^*)e^{-i2\pi c\tau/\lambda_i} + c.c., \tag{2}$$

where $c.c.$ indicates the complex conjugate and c is the speed of light. The coordinate x' is Fourier conjugate to the pixel coordinates of the camera, and can be related to the real-space coordinate by considering the wavelength-dependent resolution and shift Δ_{px}. It deserves emphasis that the *complex-valued* data $\sum_i^{N_\lambda}(p_i * r_i^*)e^{-i2\pi c\tau/\lambda_i}$ can be directly retrieved from the diffraction pattern measured at a single delay τ by spatially isolating the multi-wavelength hologram (see Fig. 1(c),(e)).

The spectroscopic reconstruction problem can therefore be posed as follows: Given $M(x',\tau_j)$ for $j \in [1, N_\tau]$, find the complex-valued $p_i^* * r_i$ for each $i \in [1, N_\lambda]$ at each x'. For suitably chosen delays τ_j, this problem is well posed, and can be solved by matrix inversion or least-squares methods. Ignoring prior knowledge of the shape of the holography sample there are at most $N_\lambda + 1$ unknown complex values for each x', indicating that at most $N_\tau = N_\lambda + 1$ measurements are required. This is reduced by 1 for sufficiently large Δ, since the autocorrelation terms can be filtered out spatially. A more dramatic reduction is achieved if the partial overlap of the monochromatic holograms is considered, as explained by the previous example.

3. Spectroscopic holography

In order to record FTSH data at EUV wavelengths, we employ an ultrastable birefringent common-path interferometer [27,34] to split the output of a 1 kHz, 35 fs, 1030 nm laser (Light Conversion Pharos, compressed by cascaded nonlinear compression in 800 mbar argon [35]) into phase-locked pulses with a controllable delay. By tilting one wedge of the common-path interferometer, these pulses are focused to two spots 200 µm apart in a Krypton gas cell, where they generate two phase-locked EUV beams. After a 200 nm Al filter to block the fundamental laser light, the high-harmonic spectrum of both pulses spans from 80 to 29 nm. At 94 cm after the HHG, we use a broadband curved multilayer mirror (f = 25 cm) to image the pulse pair onto the sample region. In the focus plane, the two EUV beams are separated by roughly 70 µm,

Optics EXPRESS

and the diameter of the individual beams is roughly 25 µm. To facilitate a more homogeneous illumination of the sample, we place the FTH sample ≈5 mm downstream of the focus. As both the reference and sample structures are illuminated by focused EUV beams, FTSH can harness the available EUV flux more efficiently than comparable spectrally resolved CDI [30]. This advantage is further increased by the use of an extended reference (here, a disk with 12 µm diameter). The EUV camera (Andor IkonL, 13.5 micron pixel size) is placed 10 cm behind the sample.

In this geometry, we now record full FTSH data. Analysis of a high-resolution FTS scan with a time-step of 23 as over a range of 11.6 fs confirms that the HHG spectrum consists of 11 high harmonics with frequencies that match to the odd harmonics 13 to 33, with a typical upper limit on the line width of 0.5 eV. The oscillation period of these harmonics ranges from 262 as to 103 as. In the following, this dataset will serve as a reference and allows to benchmark the analysis results when only using few-delay subsets of the full data.

Next, we therefore subsample the full FTS scan in order to demonstrate the minimum sampling requirements for full spectroscopic image reconstruction. Specifically, we now consider interferometric diffraction patterns at $N_\tau = N_\lambda = 11$ equidistant delays in the range 0 - 1.7 fs (step size 190 as), which corresponds to a half cycle of the driving laser pulse. By the Nyquist theorem, the spectral resolution of the Fourier transform of this data exactly matches with the spacing of the high harmonics, namely twice the fundamental frequency. However, the sampling frequency is much lower than the highest frequency in the data, and we emphasize that the spectral amplitudes cannot be reconstructed using a Fourier transform. Instead, we solve Eq. (2) using the Newton conjugate-gradient method implemented in RegPy [36,37], a Python-based toolbox for implementing and solving (potentially ill-posed) inverse problems. While the spectral reconstruction can also be achieved using other methods, this toolbox provides a number of advanced capabilities that we will exploit later.

For the case that $N_\tau = N_\lambda$, the reconstruction problem is fully constrained: for each pixel x' we have N complex-valued measurements and use these to determine N complex-valued amplitudes. This is also reflected in the measurement results: as shown in Fig. 2(b),(c), the $N_\tau = 11$ measurement allows to accurately extract the spectrally-resolved holograms from the data. This method already provides a powerful advantages over the full FTS scan: As a full FTS scan of the diffraction pattern requires to sample the highest harmonic with 2 points per oscillation and must also resolve the individual harmonics, the number of samples must be at least twice the order of the highest harmonic (i.e., 66 measurements for our spectrum with harmonics up to the 33$^{\text{rd}}$ order), the total number of measurements is dramatically reduced. In practice, the sampling advantage is around an order of magnitude, as full FTS measurements in the EUV typically use hundreds of delays. In addition to a shorter measurement time, this implies that the short scan is much less sensitive to experimental drift, such as in the EUV beam pointing.

Next, we exploit the intrinsic wavelength-sensitivity of FTH, which leads to the relative displacement of the individual spectral components that was discussed earlier. Based on the known width (30 µm) and separation (100 µm) of the sample and reference, we construct a simple mask to constrain which spectral components can contribute to each pixel x'. From this analysis, we find that at no point more than 6 high harmonics contribute to the signal (and 99% of the pixels include contributions of ≤ 5 harmonics only). We therefore set $N_\tau = 6$ and use interference patterns spaced in delay by $1.7/5 = 0.34$ fs to again cover one half cycle of the driving laser pulse. The mask can be implemented conveniently into the RegPy reconstruction method. As shown in Fig. 2(e), this approach enables spectroscopic imaging at a total measurement time of only 94 s. These results demonstrate that the temporal sampling requirements can be reduced by more than an order of magnitude compared to naive application of the Nyquist-Shannon limit, requiring in this case only 6 measurements instead of 66.

Optics EXPRESS

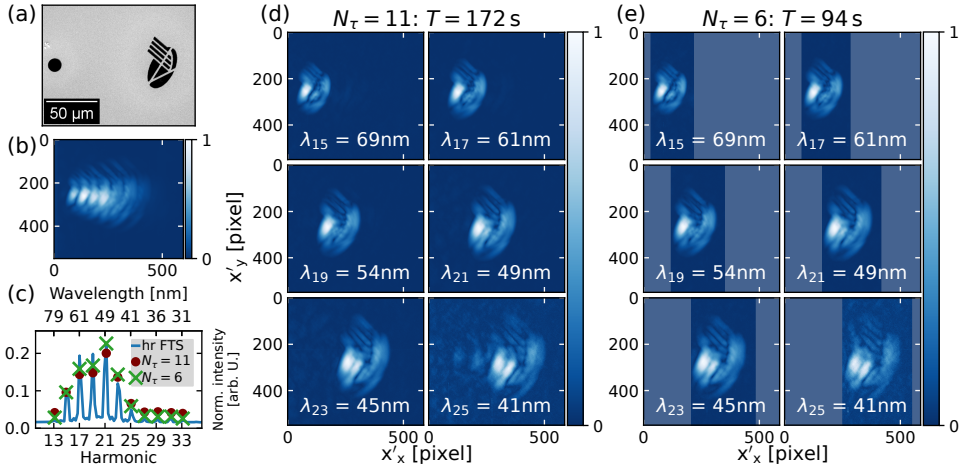

Fig. 2. Fast Fourier-transform spectroscopic holography using minimal sampling. (a) Scanning electron microscopy image of the FTH sample, which was made by focused ion beam milling of a gold-coated silicon nitride membrane. (b) Exemplary amplitude $|M(x', T)|$ of the multi-wavelength hologram, showing that the different spectral components are partially overlapping. (c) Extracted spectral intensity from the high resolution FTS scan, a dataset with $N_\tau = 11$ shots and $N_\tau = 6$ shots. The fundamental wavelength is 1030 nm. For comparison, the data was normalized to the total observed intensity. The small differences between the different datasets can be attributed to intensity drift and shot-to-shot variation in the HHG light source. (d) Spectroscopic holography results from the $N_\tau = 11$ dataset for the 6 brightest high harmonics. (e) The corresponding spectroscopic holography results from the $N_\tau = 6$ dataset. Although the resolution of these holograms is limited by the reference aperture size, they contain sufficient information to retrieve high-resolution reconstructions, as shown in Fig. 3.

4. High-resolution spectromicroscopy

A limitation of FTH is the trade-off between resolution (requiring small reference structures) and signal strength (requiring large references). This is clearly seen in Fig. 2, where the spatial resolution is strongly limited by the 12 µm reference aperture. Hence, many FTH experiments use subsequent iterative phase retrieval to improve the spatial resolution and SNR [17,18,38]. In the following, we will demonstrate how iterative image reconstruction methods can be used to achieve a resolution in FTSH that is only limited by the numerical aperture of the scattered light. In a first step, it is useful to separate the delay-dependent and delay-independent contributions to the diffraction pattern. The delay-independent part has two contributions: $\sum_i^{N_\lambda} |\tilde{p}_i|^2$ and $\sum_i^{N_\lambda} |\tilde{r}_i|^2$. These terms each represent a conventional broadband diffraction pattern, for which it is known that image reconstruction is possible with strong prior knowledge of the spectral response of the object [39]. Reconstruction of the individual spectral components, however, is not generally possible. Also, the incoherent sum of both broadband diffraction patterns will complicate image reconstruction. Consequentially, we will focus in the following on the spectrally-resolved interference patterns that are retrieved from the FTSH analysis.

After applying a Fourier transform to the output of the FTSH analysis (such as shown in Fig. 2(d),(e)), the monochromatic interference-diffraction patterns can be expressed as $m_\lambda(k) = \tilde{p}_\lambda \tilde{r}^*_\lambda(k)$. As this data already includes the phase, it is not necessary to implement phase retrieval algorithms as in monochromatic CDI. Instead, the image reconstruction of p_λ from m_λ can be posed as a deconvolution problem, where the point-spread function of the reference (r_λ) needs to be subtracted from the data. This can also be observed in the extracted monochromatic

Optics EXPRESS

far-field interference pattern (Fig. 3(a)), where a clear imprint of the Airy pattern due to the 12 micron reference can be seen. We emphasize that the clear visibility of the Airy rings is due to the direct illumination of both the reference and the sample using focused EUV beams. The shape of the observed Airy pattern matches well to the expected pattern (Fig. 3(b)) and allows us to verify the scaling of the reference aperture and the far-field propagation.

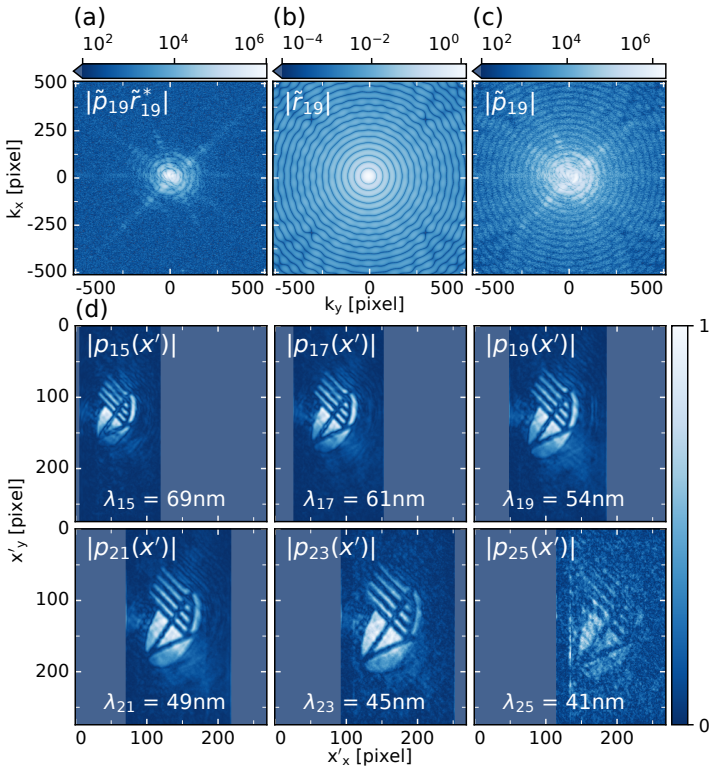

Fig. 3. Diffraction-limited spectroscopic imaging based upon the $N_\tau = 6$ dataset with a total measurement time of 1m 34s. (a) Far-field interference pattern $|\tilde{p}_\lambda \tilde{r}^*_\lambda|$ of the 19$^{\text{th}}$ harmonic at 54 nm. (b) The far-field diffraction pattern (Airy pattern) of the reference structure at 54 nm. (c) Reconstructed far-field diffraction pattern $|\tilde{p}_\lambda|$ of the object, as extracted from (a). (d) Reconstructed images for the 15$^{\text{th}}$ to 25$^{\text{th}}$ harmonics, respectively.

To reconstruct the diffraction-limited image from the monochromatic interferogram $m_\lambda(k)$ and the known reference r_λ, we use the Newton conjugate-gradient method to iteratively minimize $||\tilde{p}_\lambda \tilde{r}^*_\lambda(k) - m_\lambda(k)||$. In order to prevent overfitting to the noise, we use Morozov's discrepancy principle, i.e. we terminate the algorithm as soon as the residuals are on the order of the noise floor. This is commonly achieved after 11 to 15 Newton steps. Using this procedure, we find accurate image reconstructions for up to 6 high-harmonics, see Fig. 3, where the sample structure can now clearly be recognized. We also observe an intensity gradient and wavefront curvature that matches to the expected diverging EUV beam profile. Compared to the initial holograms that were limited by the 12 micron diameter reference, this reconstruction procedure enables a dramatic increase in the resolution to a final resolution of approximately 1.5 micron, as determined by a line scan. This resolution corresponds to the numerical aperture of the observed reference diffraction. In following experiments, the implementation of smaller or structured references, placed directly in the focus of one of the EUV beams, can enhance the intensity of the scattered light at higher numerical aperture, and thereby optimize the resolution of the ultimately

Optics EXPRESS

recovered images. The current experimental setup supports an Abbe-limited resolution of 150 nm for the 25th harmonic at 41 nm. Also, the resolution and SNR can be improved by averaging of several consecutive measurements (see Supplement 1). Finally, it is worth noting that this image reconstruction procedure does not depend on knowledge of the object support.

5. Discussion

Our results indicate that the sampling requirements in spatially-resolved Fourier transform spectroscopy, specifically when applied in combination with Fourier transform holography, is not determined by the well-known Nyquist-Shannon theorem applied to the HHG source spectrum, but it is rather determined by the total number of unknowns, which is in turn dependent on the FTH sample structure, the spectral resolution, and the bandwidth of the EUV spectrum. For typical HHG spectra spanning an octave or more and typical FTH sample structures, this leads to a significant reduction of the sampling requirements. In practice, the number of delay steps needed can be controlled by the sample-reference separation Δ. Increasing Δ at fixed sample width leads to a reduced overlap of the individual spectral components and consequentially a reduced number of steps. However, the increased Δ also implies that a larger total field of view must be considered in FTH. For diffraction-limited imaging at high numerical aperture, this can result in a reduction of the final image resolution. Thus, in general a trade-off between image acquisition speed, image quality and experimental parameters such as the illumination beamline must be found. An interactive notebook illustrating the connection between the separation Δ and the EUV spectral bandwidth can be found in Ref. [41].

To quantify the benefit of minimal sampling FTSH compared to high-resolution FTS, we carry out an analysis of the effective signal-to-noise (SNR) ratio of the reconstructed images in Fig. 4. Specifically, we compare the spectroscopic images retrieved from the $N_\tau = 6$ and $N_\tau = 11$ data sets to those from a full FTS measurement with $N_\tau = 75$. Strikingly, we observe that both the $N_\tau = 6$ and $N_\tau = 11$ show highly similar SNR to the $N_\tau = 75$ data. As exemplified in Fig. 4(c)–(e), we also find no significant differences in the retrieved image resolution. Assuming that the SNR scales with $\sqrt{T}$, where T is the total measurement time, as for shot-noise-limited data, our results indicate an improvement in the SNR for $N_\tau = 6$ of almost an order of magnitude over $N_\tau = 75$ (see Fig. 4(b)). We tentatively attribute this difference to a reduced sensitivity to drifts in the EUV spectrum and beam pointing for the shorter FTSH measurement. This conclusion is also supported by an analysis of the SNR of the spectrally resolved low-resolution holograms (based on Fig. 2(d),(e), see Fig. S4 for the SNR comparison), showing that the FTS scan yielded only marginally better holograms than minimally sampled FTSH. Thus, by enabling full spectral information within a shorter measurement time, high-quality FTSH data can be recorded straightforwardly by averaging many consecutive measurements (see Supplement 1 for an example).

The presented FTSH method relies on prior knowledge of the high-harmonic frequencies. Although these can be commonly estimated from the spectrum of the near-infrared driving pulse, the high-harmonic spectrum can be shifted due to various effects such as pulse chirp and intensity blue-shift [42,43]. Therefore, we have performed an analysis of frequency miss-estimation on the reconstructed electric fields, from which we find that a $\pm 1\%$ error in the fundamental frequency typically leads to an error of 10% (see Supplement 1, section 3). Such errors can be completely avoided, however, by performing an extended measurement with at least one extra delay. The number of independent pixels is normally much larger than the number of spectral components (10^5 pixels and 11 frequency components in our work), and thus this extra image provides enough data to determine the high-harmonic frequencies precisely through iterative minimization. With regard to the measurement calibration, also sub-wavelength accuracy is required in the determination of the delays. This can for example be achieved using a stable interferometer [34] or through separate interferometric delay calibration [44]. An advantage of

Optics EXPRESS

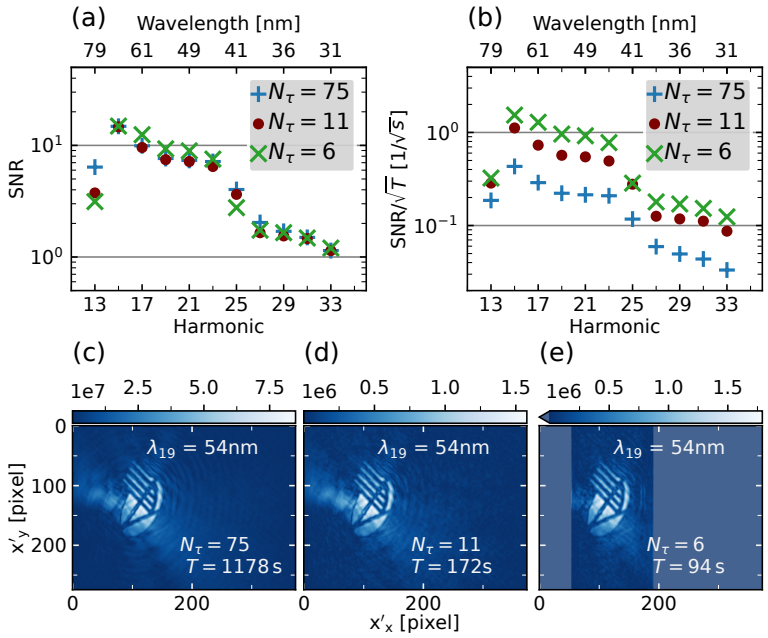

Fig. 4. Comparison of image quality for minimally sampled FTSH compared to FTS with $N_\tau = 75$ covering a delay range of 3.48 fs. This is the minimum delay range that allows to separate the individual high harmonics by a Fourier transform. (a) The experimental signal-to-noise ratio (SNR), calculated by comparing the average logo intensity to the background, shows that all three methods yield highly similar SNR despite the large difference in total exposure time. (b) Under the assumption that the SNR is dominated by shot noise, scaling the SNR by $1/\sqrt{T}$, where T is the total measurement time, enables to predict the SNR at a longer (or shorter) total exposure time. In this manner, we find that the minimally sampled FTSH method with $N_\tau = 6$ yields almost an order of magnitude better data than classical FTS. (c)-(e) Exemplary spectrally-resolved holograms for the 19$^{\text{th}}$ harmonic at 54 nm for the $N_\tau = 75$, $N_\tau = 11$, and $N_\tau = 6$ data sets, respectively. Analysis of the spectrally resolved images by line scans and decorrelation analysis [40] confirm that the spatial resolution is comparable for each of the data sets.

the minimally-sampled FTSH scheme for typical HHG spectra is that the necessary delay range covers less than one micrometer, thereby reducing the requirements on the interferometer.

Finally, we will shortly discuss the potential of FTSH for attosecond time-resolved studies. A crucial aspect here is the (quasi-)continuous EUV spectrum of attosecond EUV spectra. In the FTH multi-wavelength hologram, this leads to the superposition of a continuum of holograms [19], rather than a discrete set of wavelength components. Similarly, for HHG using few-cycle laser pulses, the broad line width of individual high harmonics can reduce the achievable resolution in diffractive imaging [39]. In either case, the delay sampling points can be adapted, extending the total time range to increase the spectral resolution as necessary. Crucially, assuming that the autocorrelation and hologram terms can be separated spatially, the number of delays N_τ is at most equal to the number of spectral components, and this can usually be reduced by considering the sample geometry and spectral bandwidth.

In summary, we have investigated the potential of Fourier-transform spectroscopic holography (FTSH), an interferometric technique that allows minute-scale spectromicroscopy at extreme ultraviolet photon energies. In the FTH geometry, prior knowledge of the illumination wavelengths allows a dramatic reduction in the sampling requirements. We have identified two sampling

Optics EXPRESS

strategies for minimally sampled FTSH: (i) without assuming prior knowledge on the overlap of monochromatic holograms, the number of measurements can be reduced to the number of wavelength components in the illumination, and (ii) by incorporating such prior knowledge, a further reduction can be achieved. For our HHG spectrum and FTH sample, this reduces the number of measurements to 6, which is a typical value. Overall, this approach enables an order of magnitude reduction in the required sampling compared to full FTS sampling by the Nyquist-Shannon theorem, thereby speeding up the measurement dramatically. In the spectrally resolved holograms, we find that a higher SNR is achieved in equivalent time. This is made possible by the shorter measurement duration that reduces the effect of long-term drift and instability in the experimental setup. Finally, although the measurement is based on holography and intrinsically measures the convolution between sample and reference, FTSH does enable high spatial resolution through iterative image reconstruction. We expect that this method will contribute strongly to the implementation of table-top extreme ultraviolet spectromicroscopy, for example in time-resolved experiments where a fast measurement is necessary to facilitate systematic studies.

Funding. European Research Council (864016); Deutsche Forschungsgemeinschaft (432680300/SFB 1456).

Disclosures. The authors declare no conflicts of interest.

The experiments were performed at ARCNL, a public-private partnership between the University of Amsterdam (UvA), Vrije Universiteit Amsterdam (VU), Rijksuniversiteit Groningen (RUG), the Dutch Research Council (NWO), and the semiconductor equipment manufacturer ASML.

Data availability. The data and python code underlying the results presented in this paper are publicly available from GRO.Data [45]. Furthermore, interactive scripts to analyze the sampling requirements in FTSH and to simulate FTSH reconstructions can be found in Ref. [41].

Supplemental document. See Supplement 1 for supporting content.

References

1. F. Krausz and M. Ivanov, "Attosecond physics," Rev. Mod. Phys. **81**(1), 163–234 (2009).
2. L. Loetgering, S. Witte, and J. Rothhardt, "Advances in laboratory-scale ptychography using high harmonic sources [Invited]," Opt. Express **30**(3), 4133–4164 (2022).
3. R. Battistelli, D. Metternich, M. Schneider, *et al.*, "Coherent x-ray magnetic imaging with 5 nm resolution," Optica **11**(2), 234 (2024).
4. M. D. Seaberg, D. E. Adams, E. L. Townsend, *et al.*, "Ultrahigh 22 nm resolution coherent diffractive imaging using a desktop 13 nm high harmonic source," Opt. Express **19**(23), 22470–22479 (2011).
5. M. Schultze, K. Ramasesha, C. Pemmaraju, *et al.*, "Attosecond band-gap dynamics in silicon," Science **346**(6215), 1348–1352 (2014).
6. F. Siegrist, J. A. Gessner, M. Ossiander, *et al.*, "Light-wave dynamic control of magnetism," Nature **571**(7764), 240–244 (2019).
7. R. Geneaux, H. J. B. Marroux, A. Guggenmos, *et al.*, "Transient absorption spectroscopy using high harmonic generation: a review of ultrafast X-ray dynamics in molecules and solids," Phil. Trans. R. Soc. A. **377**(2145), 20170463 (2019).
8. E. de Vos, S. Neb, A. Niedermayr, *et al.*, "Ultrafast Transition from State-Blocking Dynamics to Electron Localization in Transition Metal β-Tungsten," Phys. Rev. Lett. **131**(22), 226901 (2023).
9. T. Heinrich, H.-T. Chang, S. Zayko, *et al.*, "Electronic and Structural Fingerprints of Charge-Density-Wave Excitations in Extreme Ultraviolet Transient Absorption Spectroscopy," Phys. Rev. X **13**(2), 021033 (2023).
10. C. Möller, H. Probst, G. S. M. Jansen, *et al.*, "Verification of ultrafast spin transfer effects in iron-nickel alloys," Commun. Phys. **7**(1), 74 (2024).
11. H. Probst, C. Möller, M. Schumacher, *et al.*, "Unraveling femtosecond spin and charge dynamics with extreme ultraviolet transverse MOKE spectroscopy," Phys. Rev. Res. **6**(1), 013107 (2024).
12. A. S. Johnson, J. V. Conesa, L. Vidas, *et al.*, "Quantitative hyperspectral coherent diffractive imaging spectroscopy of a solid-state phase transition in vanadium dioxide," Sci. Adv. **7**(33), eabf1386 (2021).
13. A. S. Johnson, D. Perez-Salinas, K. M. Siddiqui, *et al.*, "Ultrafast X-ray imaging of the light-induced phase transition in VO_2," Nat. Phys. **19**, 215–220 (2023).
14. I. McNulty, J. Kirz, C. Jacobsen, *et al.*, "High-Resolution Imaging by Fourier Transform X-ray Holography," Science **256**(5059), 1009–1012 (1992).
15. H. He, U. Weierstall, J. C. H. Spence, *et al.*, "Use of extended and prepared reference objects in experimental Fourier transform x-ray holography," Appl. Phys. Lett. **85**(13), 2454–2456 (2004).

Optics EXPRESS

16. S. Marchesini, S. Boutet, A. E. Sakdinawat, *et al.*, "Massively parallel X-ray holography," Nat. Photonics **2**(9), 560–563 (2008).
17. V. T. Tenner, K. S. E. Eikema, and S. Witte, "Fourier transform holography with extended references using a coherent ultra-broadband light source," Opt. Express **22**(21), 25397–25409 (2014).
18. J. Geilhufe, B. Pfau, C. M. Günther, *et al.*, "Achieving diffraction-limited resolution in soft-X-ray Fourier-transform holography," Ultramicroscopy **214**, 113005 (2020).
19. W. Eschen, S. Wang, C. Liu, *et al.*, "Towards attosecond imaging at the nanoscale using broadband holography-assisted coherent imaging in the extreme ultraviolet," Commun. Phys. **4**(1), 154 (2021).
20. S. Zayko, O. Kfir, M. Heigl, *et al.*, "Ultrafast high-harmonic nanoscopy of magnetization dynamics," Nat. Commun. **12**(1), 6337 (2021).
21. P. Thibault, M. Dierolf, A. Menzel, *et al.*, "High-Resolution Scanning X-ray Diffraction Microscopy," Science **321**(5887), 379–382 (2008).
22. B. Zhang, D. F. Gardner, M. H. Seaberg, *et al.*, "Ptychographic hyperspectral spectromicroscopy with an extreme ultraviolet high harmonic comb," Opt. Express **24**(16), 18745–18754 (2016).
23. A. Rana, J. Zhang, M. Pham, *et al.*, "Potential of Attosecond Coherent Diffractive Imaging," Phys. Rev. Lett. **125**(8), 086101 (2020).
24. L. Loetgering, X. Liu, A. C. C. D. Beurs, *et al.*, "Tailoring spatial entropy in extreme ultraviolet focused beams for multispectral ptychography," Optica **8**(2), 130–138 (2021).
25. D. Descamps, C. Lyngå, J. Norin, *et al.*, "Extreme ultraviolet interferometry measurements with high-order harmonics," Opt. Lett. **25**(2), 135–137 (2000).
26. M. Kovačev, S. V. Fomichev, E. Priori, *et al.*, "Extreme Ultraviolet Fourier-Transform Spectroscopy with High Order Harmonics," Phys. Rev. Lett. **95**(22), 223903 (2005).
27. G. S. M. Jansen, D. Rudolf, L. Freisem, *et al.*, "Spatially resolved Fourier transform spectroscopy in the extreme ultraviolet," Optica **3**(10), 1122–1125 (2016).
28. Y. Meng, C. Zhang, C. Marceau, *et al.*, "Octave-spanning hyperspectral coherent diffractive imaging in the extreme ultraviolet range," Opt. Express **23**(22), 28960–28969 (2015).
29. S. Witte, V. T. Tenner, D. W. Noom, *et al.*, "Lensless diffractive imaging with ultra-broadband table-top sources: from infrared to extreme-ultraviolet wavelengths," Light: Sci. Appl. **3**(3), e163 (2014).
30. G. S. M. Jansen, A. C. C. d. Beurs, X. Liu, *et al.*, "Diffractive shear interferometry for extreme ultraviolet high-resolution lensless imaging," Opt. Express **26**(10), 12479–12489 (2018).
31. G. O. Williams, A. I. Gonzalez, S. Künzel, *et al.*, "Fourier transform holography with high harmonic spectra for attosecond imaging applications," Opt. Lett. **40**(13), 3205–3208 (2015).
32. S. G. Kalenkov, G. S. Kalenkov, and A. E. Shtanko, "Hyperspectral holography: an alternative application of the Fourier transform spectrometer," J. Opt. Soc. Am. B **34**(5), B49–B55 (2017).
33. A. Genco, C. Cruciano, M. Corti, *et al.*, "k-Space Hyperspectral Imaging by a Birefringent Common-Path Interferometer," ACS Photonics **9**(11), 3563–3572 (2022).
34. D. Brida, C. Manzoni, and G. Cerullo, "Phase-locked pulses for two-dimensional spectroscopy by a birefringent delay line," Opt. Lett. **37**(15), 3027–3029 (2012).
35. M.-S. Tsai, A.-Y. Liang, C.-L. Tsai, *et al.*, "Nonlinear compression toward high-energy single-cycle pulses by cascaded focus and compression," Sci. Adv. **8**(31), eabo1945 (2022).
36. M. Hanke, "Regularizing properties of a truncated newton-cg algorithm for nonlinear inverse problems," Numerical Functional Analysis and Optimization **18**(9-10), 971–993 (1997).
37. S. Maretzke, M. Bartels, M. Krenkel, *et al.*, "Regularized newton methods for x-ray phase contrast and general imaging problems," Opt. Express **24**(6), 6490–6506 (2016).
38. F. Capotondi, E. Pedersoli, M. Kiskinova, *et al.*, "A scheme for lensless x-ray microscopy combining coherent diffraction imaging and differential corner holography," Opt. Express **20**(22), 25152–25160 (2012).
39. J. Huijts, S. Fernandez, D. Gauthier, *et al.*, "Broadband coherent diffractive imaging," Nat. Photonics **14**(10), 618–622 (2020).
40. A. Descloux, K. S. Grußmayer, and A. Radenovic, "Parameter-free image resolution estimation based on decorrelation analysis," Nat. Methods **16**(9), 918–924 (2019).
41. "CRC 1456 / LiveDocs / RG - EUV spectroscopic imaging GitLab," (2024). https://gitlab.gwdg.de/crc1456/livedocs/rg-euv-spectroscopic-imaging.
42. Z. Chang, A. Rundquist, H. Wang, *et al.*, "Temporal phase control of soft-x-ray harmonic emission," Phys. Rev. A **58**(1), R30–R33 (1998).
43. H. J. Shin, D. G. Lee, Y. H. Cha, *et al.*, "Nonadiabatic blueshift of high-order harmonics from Ar and Ne atoms in an intense femtosecond laser field," Phys. Rev. A **63**(5), 053407 (2001).
44. Y. Meng, C. Zhang, C. Marceau, *et al.*, "Interferometric time delay correction for Fourier transform spectroscopy in the extreme ultraviolet," J. Mod. Opt. **63**(17), 1661–1667 (2016).
45. G. S. M. Jansen and H. Strauch, "Replication Data for: Fast spectroscopic imaging using extreme ultraviolet interferometry," GRO.data (2024), https://doi.org/10.25625/YA0MNQ.